Title
MICROSTRUCTURE AND PROPERTIES OF RARE EARTH MAGNETS

Author
Ramesh, R.

Publication Date
1987-11-01

Lawrence Berkeley Laboratory
UNIVERSITY OF CALIFORNIA

Materials & Chemical Sciences Division

Presented at the ASM Symposium on Hard and Soft Magnetic Materials with Applications, Cincinnati, OH, October 10–14, 1987

Microstructure and Properties of Rare Earth Magnets

R. Ramesh, J.K. Chen,
L.K. Rabenberg, and G. Thomas

November 1987

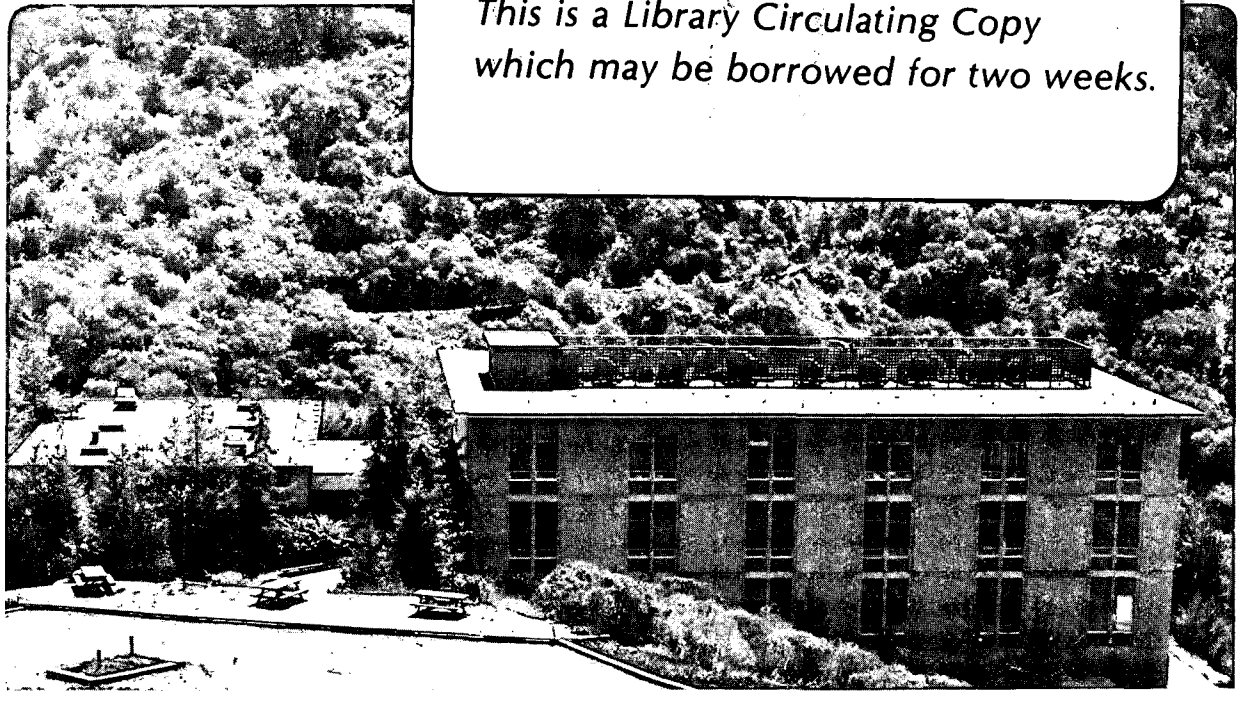

Prepared for the U.S. Department of Energy under Contract DE-AC03-76SF00098

DISCLAIMER

EFFECT OF QUENCH RATE ON THE INTRINSIC COERCIVITY OF IRON/RARE EARTH/BORON PERMANENT MAGNETS

R.RAMESH and G.THOMAS#

Department of Materials Science and Mineral Engineering and Materials and Chemical Sciences Division, Lawrence Berkeley Laboratory, University of California, Berkeley, CA 94720.

Scientific Director, National Center for Electron Microscopy, Lawrence Berkeley Laboratory, University of California, Berkeley, CA 94720.

ABSTRACT : The effect of post-sintering cooling rate on the microstructure and magnetic properties of Fe-Nd-B based magnets has been studied. It has been shown that the intrinsic coercivity and energy product vary inversely as the cooling rate. In all the cases, the magnet behaves as a nucleation controlled magnet characterized by a high initial permeability, although nucleation of reverse domains occurs at progressively lower fields as the cooling rate is increased. Samples quenched into water and oil exhibited extensive intergranular quench cracking. Scanning Auger elemental mapping as well as energy dispersive xray microanalysis showed the presence of oxygen, along with the rare earths, in the grain boundary phase. A qualitative argument for the influence of oxygen in reducing the magnetocrystalline anisotropy of the $RE_2Fe_{14}B$ phase is presented. Finally, the effect of cooling rate on the intrinsic coercivity and energy product can be understood in terms of the effect of local strains, at the grain boundaries and interfaces, on the magnetocrystalline anisotropy of the $RE_2Fe_{14}B$ phase.

INTRODUCTION : Ever since the discovery of the phase $Nd_2Fe_{14}B$[1,2], there have been a large number of investigations[3] aimed at understanding the origin of the record high hard magnetic properties of this system and also the cause for the changes in the intrinsic coercivity with thermal treatments. The excellent permanent magnetic properties of this system are primarily due to the large saturation magnetization (1.61 T at room temperature) of $Nd_2Fe_{14}B$ coupled with a moderately high anisotropy field of 70 kOe at room temperature, although the Curie temperature(312^oC) is low compared to the $SmCo_5$ magnets(830^oC). Permanent magnets have been prepared by both the P/M sintering route[4] as well as by melt-spinning[5]. In this paper, magnets prepared by the former technique have been examined. These sintered magnets belong to the class of magnets termed as " nucleation-controlled" magnets. In such magnets, the reversal of magnetization of each grain is accomplished by the nucleation and movement of domain walls to reverse the magnetization of a fully saturated grain. In "nucleation-controlled" magnets, the nucleation field[6] (value of the total field at which reversal starts) is controlled predominantly by the nucleation step. In Fe-Nd-B magnets, the exact details of the nucleation process are still unclear, although it is generally accepted that nucleation in the bulk of the magnet occurs at internal interfaces such as grain boundaries or two-phase interfaces. Some suggested mechanisms include (i) the effect of quenching stresses ; (ii) the presence of a soft magnetic bcc phase at the grain boundaries[7] ; (iii) the role of oxygen in providing regions of lowered anisotropy[8]. However, no conclusive mechanism has been proposed so far that will explain not only the changes in intrinsic coercivity with thermal treatments but also the fact that the highest intrinsic coercivity is much lower than the anisotropy field, H_A of 70kOe. Since the magnetic properties are

extremely sensitive to changes in the microstructure, it is consequently important to characterize the microstructure and correlate their changes to those of the magnetic properties.

The microstructure of sintered magnets has been investigated in some detail in earlier papers[9-13] and has been summarized by Livingston[14]. As shown schematically in Fig.1, the microstructure consists of large (about 10μm) grains of almost defect free $Nd_2Fe_{14}B$, at the triple grain junctions of which a rare-earth rich fcc phase has been observed. Electron microscopy studies[9-11] show that the spatial extent of this phase varies from a few microns at the triple junctions, to a few tens of nanometers at the two-grain boundaries. It was also shown that the fcc structure arises due to the presence of oxygen in this phase[9]. The role of this phase, especially the oxygen in it, in the magnetization reversal process is still unclear. In addition, a $Nd_{1+x}Fe_4B_4$ phase has also been found as independent grains . This phase is paramagnetic at room temperature and is not considered to be a useful constituent. Likewise,due to improper processing, hexagonal rare earth oxides have also been observed in these TEM investigations[11].

Earlier investigations have focussed on the effect of post-sintering heat treatment upon the intrinsic coercivity and energy product, $(BH)_{max}$[4,15-19]. In the as-water quenched condition, the intrinsic coercivity and $(BH)_{max}$ are low. However, upon annealing at 500-600^oC for one hour, the intrinsic coercivity is almost tripled along with a considerable increase in the $(BH)_{max}$. This is clearly shown in Fig.2 which shows the intrinsic coercivity as function of annealing temperature for a typical magnet which has been water quenched. It has also been shown that a high intrinsic coercivity can be obtained by slow cooling from sintering temperature to room temperature[20].

With this as background, the present set of experiments were undertaken to examine the effect of post-sintering cooling rate upon the magnetic properties and microstructure of a typical sintered magnet. The rationale behind such a set of experiments was that if quenching stresses do indeed influence the intrinsic coercivity, then the cooling rate from the sintering temperature would have a significant influence upon the intrinsic coercivity. Also if the quenching process alters the microstructure significantly then the magnetic properties should also be influenced. Thus the microstructure of the magnets with different quenching rates was also examined and characterized employing various analytical techniques.

EXPERIMENTAL: The nominal alloy composition studied was Fe-32.5wt.% rare earth-1wt.% B wherein the rare earth composition was 5% Ce-15%Pr-80%Nd. The magnets were prepared by a standard powder metallurgical technique[2,4]. In the case of the quench rate experiments, the samples were quenched from the sintering temperature into various media such as water, silicone oil, flowing Argon etc. to obtain different cooling rates.

Magnetic Measurements : Magnetic measurements were carried out on cylindrical samples (1cm x 1cm) using a hysteresigraph. A maximum field of 20kG was applied to study the hysteresis loops as well as the nature of the virgin curve. All measurements were carried out at room temperature. The samples were characterized using a variety of techniques. Scanning electron microscopy of the samples was carried out to examine the effect of various cooling rates upon the structural integrity of the magnets, e.g., the presence of microcracks on the surfaces. Samples for Transmission Electron Microscopy(TEM) were prepared by sectioning a thin wafer from the bulk magnet, mechanical thinning anf finally Argon ion milling to electron transparency at 6kV with a beam current of 0.3-0.4 mA,

corresponding to a specimen current of 30-40μA. Conventional imaging and Analytical Electron Microscopy (AEM) were carried out in a Philips 400 TEM/STEM at 100kV. Detection of oxygen was accomplished using an ultra-thin window detector on a 200kV JEOL microscope at the National Center for Electron Microscopy. Care was taken to ensure statistical significance of the xray microanalytical data by acquiring at least 10^5 counts. Spectral deconvolution and quantification was carried out using theoretically generated k-factors. However, in the case of oxygen experimentally corrected values of k-factors were used. Microanalysis line profiles were carried out at various regions in many samples in order to obtain a reasonable degree of reliability of the data. High resolution TEM was carried out on a JEOL 200CX at 200kV.

Auger electron spectroscopy (AES) and elemental mapping was carried out using a Phi Scanning Auger Microscope(SAM). Standard samples were prepared and were fractured in-situ in a vacuum of 10^{-9} torr. Both point analyses as well as elemental mapping were carried out. In addition, depth profiling was also carried out to study the composition as a function of depth.

RESULTS : Fig.3 shows the intrinsic coercivity and $(BH)_{max}$ as a function of cooling rate. The values of cooling rates were determined from parallel experiments on alloy steels. As is evident, there is a definite influence of cooling rate from the sintering temperature upon the microstructure sensitive magnetic properties. The remanence , however, is independent of the cooling rate, as would be expected, since it is fixed by the starting alloy composition. This strong dependence of intrinsic coercivity and $(BH)_{max}$ on the cooling rate indicates that quenching stresses, which also increase with increasing cooling rate[21], may play a significant role in aiding nucleation of reverse domains at the grain boundaries and/or two

phase interfaces. The hysteresis curve and virgin magnetization plot for each of the cooling rates is shown in Fig.4 (a-d). The steep rise in the virgin curve, in all cases,indicates that the domain walls in the magnet can move very easily under small applied fields. Although the shape of the hysteresis loop still remains the same, nucleation is occurring at progressively lower fields as the cooling rate is increased.

Figs.5(a &b) show SEM images of the surface of the water cooled sample and the furnace cooled sample. The quench cracks on the surface of the water quenched sample are clearly visible. No such cracks were observed on the furnace cooled sample. This again supports the idea that quenching stresses can be significant in explaining the lowering of intrinsic coercivity with increased cooling rate. The fracture mode in the water quenched sample was examined by carefully opening up one of the cracks on the surface and examining it immediately under the SEM. Figs. 6(a&b) show typical examples. In Fig.6(a) a lower magnification fractograph shows almost completely intergranular fracture, which is more clearly illustrated in the higher magnification image in Fig.6(b). These results show the weakness of the grain boundaries. Similar observations have been made by Doser and Smeggil[22] in the case of Sm-Co alloys.

Microstructural characterization and microanalysis was accomplished by AES/SAM and TEM/AEM. The fracture surface of the in-situ fracture sample of a notched water quenched sample in the SAM was examined for the presence of various elements. Primarily, the surface was examined for the presence of oxygen, since in an earlier paper it was reported that in the slowly cooled condition, the grain boundaries contained significant amounts of oxygen[9]. The fracture surface, shown in Fig.7(a) is predominantly intergranular, although transgranular cleavage regions can be clearly recognized. It must be pointed out that this is not in contradiction to the result presented in Fig.6(a&b) where the fracture is due to quenching stresses, while in this case, the nature of the stresses is

due to the notch in the sample (the stress concentrator to enable fracture). Also note that transgranular fracture occurs only in regions of large grains (as shown by the arrows). Fig.8(a) shows an Auger spectrum from the intergranular region, while the peak to peak ratios as a function of sputtering time are shown in Fig.8(b). Figs.9(a & b) show the corresponding plots for the transgranular facet. The main point to be noted in Fig.9 (a) is that there is a large oxygen edge in the intergranular region. This is not superficially adsorbed oxygen, since the depth profile indicates a significant peak to peak ratio for sputtering times of upto 5 minutes. On the other hand, the transgranular region exhibits only superficially adsorbed oxygen to the extent of about 60 seconds sputtering time (equivalent to about 30Å). The oxygen and Nd Auger electron maps are shown in Figs.7(b & c) and clearly show that oxygen co-segregates with Nd in the grain boundary regions. Thus, it is possible that the predominantly intergranular fracture observed can be caused by oxygen embrittlement possibly associated with the rare earth elements as oxides. The importance of this inference in the elucidation of the magnetization reversal mechanism will be discussed later in this paper.

The effect of grain boundary segregation of oxygen and/or nitrogen on the mechanical properties of intermetallics has been extensively studied by Westbrook and co-workers[23,24]. In their case, a prominent local hardening coupled with intergranular fracture was correlated to the presence of a stoichiometric excess of the electro-positive element in the inter-metallic as well as the co-segregation of oxygen and/or nitrogen to the grain boundaries.

Some of the microstructural details of the sintered magnets have been already discussed in earlier papers[7-12]. With the use of an analytical electron microscope fitted with an ultra-thin window Energy Dispersive Xray (EDX) detector, it was possible to detect oxygen in the grain boundary Nd-rich phase, thus independently verifying the SAM results. Fig.10(a)

shows a typical EDX spectrum from the grain boundary phase. The low energy end is shown in Fig.10(b), for a water quenched sample, wherein the oxygen peak can be clearly observed. Thus, along with the Auger data, it is now established that oxygen is an integral part of the grain boundary phase, both in the water quenched sample as well as in the slowly cooled samples [ref.(8)]. Microanalysis line profiles for Ce, Pr, Nd and Fe did not show any significant difference between the water quenched sample and the slow cooled sample. Fig.11(a) shows a typical line profile across the matrix-triple junction fcc phase interface, in the case of a slow cooled sample, while Fig.11(b) shows the same for a water quenched sample. Although the fcc phase is enriched in Ce and Pr, there is no significant difference between the two samples. Samples quenched into oil or air cooled did not show any different microanalytical behaviour with respect to Ce, Pr, and Nd.

DISCUSSION :

The actual cause of magnetization reversal in this class of magnets is still unclear, although the overall behaviour is consistent with that of a nucleation controlled magnet. In a recent paper[8], it was indicated that oxygen in the grain boundary phase could play a significant role in reducing the magnetocrystalline anisotropy close to the interfaces. Another proposed mechanism attributed the nucleation of reverse domains to the presence of a soft magnetic bcc phase at the grain boundaries[7]. However, during the course of this investigation, it was conclusively demonstrated that no bcc phase exists at the grain boundaries. When observed it has been shown to be due to an artefact of Argon ion beam specimen preparation[9]. Fig.12 is a typical high resolution lattice fringe image, in the case of a water quenched sample, where the interface between the matrix $RE_2Fe_{14}B$ phase and the grain boundary fcc phase has been imaged. Clearly, no third phase is observed between the matrix phase and the fcc phase. Thus, the other two possible mechanisms, i.e., effect of oxygen and

the effect of quench rate will be considered in detail.

The role of oxygen and that of quench rate are likely to be synergistic in nature. However, even in samples which are cooled very slowly (50^{o}C/hour) the intrinsic coercivity(9.8kOe) is much below the anisotropy field (~70 kOe at room temperature for $Nd_2Fe_{14}B$), indicating that easy wall nucleation occurs at sites of considerably lowered magnetocrystalline anisotropy or higher demagnetizing fields. It is in this context that the role of oxygen has to be examined in detail. Thus, in what follows, a qualitative argument will be presented to explain the role of oxygen in aiding wall nucleation.

Consider a grain of $Nd_2Fe_{14}B$ in an aligned polycrystalline magnet. The magnetization reversal of this grain will be governed primarily by the defect configuration on its surface and the demagnetizing field. In this analysis, oxygen at the grain boundaries and in the fcc phase/ matrix phase interface is considered as one of the defects. Consider, specifically, a unit cell of the $Nd_2Fe_{14}B$ phase[1], shown in Fig.13, at the surface of the grain. The environment of this unit cell is different in different directions. The Nd atoms of this unit cell will be in close contact with the oxygen atoms in the grain boundary phase. Let an oxygen atom be located at an arbitrary position, close to the Nd atom in this unit cell, as depicted in Fig.13. Due to the large electro-negativity of oxygen, there will be a definite tendency for the oxygen atoms to draw the electrons from the Nd atoms towards itself. Since at least 2/3 of the magnetocrystalline anisotropy of the $Nd_2Fe_{14}B$ phase comes from the Nd sub-lattice, any changes in the electronic structure of the Nd atom in the unit cell will bring about large changes in the magnetocrystalline anisotropy of the crystal. This effect of oxygen can be visualized to occur in another way. The Nd atom could be visualized as being oxidized by the oxygen atom, thus, effectively removing it from the unit cell. This could

then be the cause for the drop in magnetocrystalline anisotropy. A similar mechanism has been used by Jin et. al[25] who have considered the magnetocrystalline anisotropy of Sm^{+3} near point defects in $SmCo_5$ and in Sm_2Co_{17}. Their results indicate that in some cases, significantly lowered anosotropy could be observed for defect structures. This combined with the local demagnetizing fields, will lead to easy domain wall nucleation. Rigorous application of such a model to the case of Fe-Nd-B magnets , however, must await theoretical computations of the effect of the presence of oxygen in the neighbourhood, upon the magnetocrystalline anisotropy of $Nd_2Fe_{14}B$.

The post-sintering quench rate has a definite influence upon the intrinsic coercivity, the B-H loop and thus on the energy product. Since the intrinsic coercivity decreases to a value much lower than the slowly cooled sample, some other mechanism , in addition to the effect of oxygen, must be envisaged. The SEM studies of the quenched samples clearly show that on increasing the cooling rate to above that of an oil quench, quench cracks proliferate the magnet. The presence of these cracks suggest two inferences : (1) the stresses (at least locally) are well above the fracture stress of the $Nd_2Fe_{14}B$ phase or (2) the failure stress of the interface of the matrix phase and the grain boundary phase. However, the observation of a predominantly intergranular fracture (Figs. 6(a &b)) indicates that the second case is more likely. In addition, the results of Auger elemental mapping as well as x-ray microanalysis indicate that the intergranular fracture is likely to be aided by the presence of oxygen in the grain boundary phase.

In general, the intrinsic coercivity, iHc, for a nucleation type magnet can be written as : $iHc = c.H_A - N_d.M_s$[26], where, H_A is the anisotropy field of the main magnetic phase ; c is a constant which depends upon the

nature of the nucleation sites ; N_d is the demagnetization constant which is dependent upon the shape of the grains and the degree of interaction across grain boundaries and two-phase interfaces ; M_s is the saturation magnetization. However, the anisotropy field will be strongly influenced by local changes in composition, local lattice strains, especially near grain boundaries and two-phase interfaces, which are the most likely sites of initiation of magnetization reversal by domain wall nucleation. Thus, an effective value of the anisotropy field must be used in the determination of the intrinsic coercivity. These considerations show that two properties, i.e., the effective anisotropy field and the saturation magnetization will influence the value of intrinsic coercivity, for given values of "c" and N_d.

If the quenching stresses are sufficient to cause cracking or microcracking of the polycrystalline magnet, then it is possible that the demagnetizing fields at the cracked surfaces will be important. This is because, cracking causes the formation of free surfaces, at which free poles will arise. These free poles will lead to high local demagnetizing fields. However, the effect of such a phenomenon appears to be insignificant in the case of water quenched samples. This can be shown from the results of two experiments. In the first, a strong effect of post-quench anneal on the intrinsic coercivity is observed experimentally (as was shown in Fig.2). Thus, if the sample is annealed at 500-600^{o}C for one hour the iHc can be raised to almost that of the slow-cooled sample. However, if quench crack induced demagnetizing fields are the main cause for the drop in iHc, then the annealing treatment should not show an increase in iHc, since the cracks will still remain on annealing. The second evidence which rules out the idea that internal quench cracks induced demagnetizing fields are the cause for the drop in iHc is the results of applied field dependence of iHc.

In general, for nucleation controlled magnets, a strong dependence of iHc upon the applied external field is observed[27]. At low external fields, the iHc is low since, the demagnetizing field is large enough to retain the domain walls in the grains and hence prevents saturation of the grains. Since domain walls already exist in the grains, they can easily move back and forth, since the grains themselves are almost defect free. Hence the intrinsic coercivity is low. As the field is increased to above the demagnetizing field value, the domain walls are progressively pushed out of the grains thus saturating the magnetization of the grains along the applied field direction. In this case, in order to cause reversal of the magnetization of the grains, a domain wall has to be nucleated. since this is difficult, the intrinsic coercivity is high. Thus, the effective demagnetizing field can be determined from a plot of intrinsic coercivity versus applied field, H_{app}. The value of applied field at which a sharp rise in intrinsic coercivity is noted corresponds to the effective demagnetizing field of the ensemble of grains. If quench cracks induced demagnetizing field is of significance in the case of the water quenched sample, the iHc- H_{app} plot should be different from the slow cooled sample and the quenched and annealed sample. That this is not so is clearly shown in Fig.14. This figure shows iHc versus H_{app} for : (1) the water quenched sample ; (2) the water quenched and annealed sample ; (3) the slowly cooled sample. There is no significant difference between the three samples in terms of the value of H_{app} at which iHc begins to rise (the effective demagnetizing field). Thus, in the case of the samples examined, the effect of demagnetizing field due to internal quench cracks does not appear to be the dominant cause for the drop in iHc with cooling rate, although quench cracks are observed.

Thus, it is clear that the other parameter, i.e. the effective anisotropy field, near the interfaces must be examined in detail. Specifically , the

effect of local composition , especially oxygen, and the effect of localized strains, primarily due to quenching, on the magnetocrystalline anisotropy and the effective anisotropy field need further examination. Theoretical and experimental estimations of these effects are currently under way.

CONCLUSIONS : In conclusion it has been shown that post-sintering cooling rates have a definite influence on the intrinsic coercivity and energy product of Iron-Rare Earth-Boron magnets. After water quenching, the intrinsic coercivity was found to be lower than in a slowly cooled magnet. Concurrently, the water quenched sample was proliferated with intergranular quench cracks, indicating that quenching stresses are significant. No specific differences in microanalytical details of the rare earth elements in the matrix and grain boundary phase and their interface was observed for the different cooling rate samples. From the similar field dependence of intrinsic coercivity in the different cooling rate magnets, it is shown that demagnetization fields at quench cracks is not the main cause for the difference in intrinsic coercivity for the different cooling rates. A qualitative argument for the influence of oxygen in reducing the magnetocrystalline anisotropy field of the $RE_2Fe_{14}B$ phase has been put forth to explain the low value of intrinsic coercivity compared to the anisotropy field, even in a slowly cooled sample. Finally, it is possible that local strains at the grain boundaries and two-phase interfaces could cause a large reduction in the magnetocrystalline anisotropy of the $RE_2Fe_{14}B$ phase, thus leading to an even lower intrinsic coercivity in the quenched magnet.

ACKNOWLEDGEMENTS : The authors wish to thank Professor M.Okada, Tohuku University, Japan for kindly providing the alloys used in this study. The authors also wish to acknowledge Professor W.A.Soffa for stimulating

discussions on this subject. This work was supported by the Director, Office of Basic Energy Research, Office of Basic Energy Sciences, Materials Sciences Division of the U.S. Department of Energy under contract No. DE-AC03-76SF00098.

REFERENCES

1. J.F.Herbst, J.J.Croat, F.E.Pinkerton and W.B.Yelon, Phys. Rev.B,29,4176(1984).

2. M.Sagawa, S.Fujimura, H.Yamamoto, Y.Matsuura and K.Hiraga, IEEE Trans. Magnetics, Mag -20, 1584(1984).

3. See for example Proc. of Intermag 1984, 1985, 1986 and 1987; Proc. Annual MMM Conf. 1984, 1985, 1986.

4. M.Sagawa, S.Fujimura, N.Togawa, H.Yamamoto and Y.Matsuura, J. Appl. Phys., 55, 2083(1984).

5. R.W.Lee, E.G.Brewer and N.A.Schaffel, IEEE Trans. Magnetics, Mag-21, 1958(1985).

6. J.D.Livingston, Paper No. AC-06, Intermag-1987, Tokyo, Japan.

7. K.Hiraga, M.Hirabayashi, M.Sagawa and Y.Matsuura, Japanese J. Appl. Phys.,24, L30(1985); K.Hiraga, M.Hirabayashi, M.Sagawa and Y.Matsuura, Jap. J. of Appl. Phys., 24, 699(1985).

8. R.Ramesh, G.Thomas, M.Okada and M.Homma, Paper No.AC-07, Intermag 1987, Tokyo, Japan.

9. R.Ramesh, J.K.Chen and G.Thomas, J. Appl. Phys. 61, 2993(1987).

10. R.K.Mishra, J.K.Chen and G.Thomas, J. Appl. Phys. 59, 2244(1986).

11. R.Ramesh, K.M.Krishnan, E.Goo, G.Thomas, M.Okada and M.Homma, J. Magnetism and Magnetic Materials, 54-57, 563(1986).

12. M.Tokunaga, M.Tobise, N.Meguro and H.Harada, IEEE Trans. Magnetics, Mag-22, 904(1986).

13. P.Schrey, IEEE Trans. Magnetics, Mag-22, 913(1986).

14. J.D.Livingston, Proc. of ASM Symposium on Soft and Hard Magnetic Materials, Ed. J.A.Salsgiver et. al., October, 1986.

15. M.Tokunaga, N.Meguro, M.Endoh, S.Tanigawa and H.Harada, IEEE Trans. Magnetics,Mag-21, 1964(1985).

16. T.Bailey and I.R.Harris, J. Materials Science Letters, 4, 151(1985).

17. S.Z.Zhou, L.Li, L.D.Zhang and Q.Hu, J Magnetism and Magnetic Materials, 54-57, (1986).

18. S.E.Hsu, K.L.Wang and L.C.Su, Paper No.CC-04, Intermag 1987, Tokyo, Japan.

19. J.Ormerod, J. Less Common Metals, 111, 49(1985).

20. M.Okada, S.Sugimoto, C.Ishizaka, T.Tanaka and M.Homma, J. Appl. Phys., 57, 4146(1985).

21. H.Hencke, J.R.Thomas, Jr. and D.P.H.Hasselmann, J. American Ceramics Society, 67, No.6, 393(1984).

22. M.Doser and J.G.Smeggil, IEEE Trans. Magnetics, Mag-9, 168(1973).

23. J.H.Westbrook and D.L.Wood, J. Inst. of Metals, 91, 174(1962).

24. A.U.Seybolt and J.H.Westbrook, Acta Met., 12, 449(1964).

25. H.M.Jin, H.N.Chen, D.S.Tang, J.F.Han and Y.Shi, Proc. of Sixth Int. Workshop on Rare Earth Permanent Magnets and their applications, Ed. J.Fidler, 549(1982).

26. G.Herzer, W.Fernengel and E.Adler, J. Magnetism and Magnetic Materials, 58, 48(1986).

27. J.J.Becker, J.Appl. Phys., 39, 1270(1968).

FIGURE CAPTIONS

Figure 1 : A schematic representation of the general microstructure of sintered Fe-Nd-B magnets.

Figure 2 : Effect of isochronal post-sintering annealing on the intrinsic coercivity of a typical water quenched sintered Fe-Nd-B magnet.

Figure 3 : Effect of post-sintering cooling rate on the intrinsic coercivity and energy product of Nd-Pr-Ce-Fe-B magnet.

Figure 4 : Virgin curve and corresponding hysteresis loop of Fe-Nd-Pr-Ce-B magnet cooled in different media. The maximum applied field in each case was 25 kG.

Figure 5 : (a) Scanning elctron micrograph of the polished surface of a water quenched sample ; (b) scanning electron micrograph of the polished surface of a furnace cooled sample (50^{o}C/hour).

Figure 6 : (a) Low magnification scanning electron micrograph of the fracture surface of the water quenched sample, showing a predominantly inter-granular fracture ; (b) higher magnification image of the region in (a), showing the inter-granular fracture more clearly.

Figure 7 : (a) Fracture surface of in-situ fractured Auger sample ; (b) Oxygen Auger elctron map of the region in (a) ; (c) Nd-Auger electron map of the region in (a).

Figure 8 : (a) Auger spectrum from transgranular fracture region (region A in Fig.7(a)); (b) O, Fe and Nd peak-to-peak ratios as a function of sputtering time. Note the sharp drop in the oxygen peak-to-peak ratio after

about 60 seconds of milling.

Figure 9 : (a) Auger spectrum from inter-granular fracture region (region (B) in Fig.7(a)); (b) O, Fe and ND peak-to-peak ratios as a function of milling time. Note the significant oxygen peak-to-peak ratio even after five minutes of milling.

Figure 10 : (a) A typical EDX spectrum from the grain boundary phase, obtained using an ultra-thin window(UTW) EDX detector ; (b) the low energy end of the spectrum showing the oxygen peak clearly.

Figure 11 : (a)A Typical line profile across the matrix -triple junction fcc phase interface in a slow cooled sample ; (b) a similar profile in the case of a water quenched sample.

Figure 12 : High resolution lattice fringe image of the interface between the matrix and the grain boundary fcc phase in a water quenched sample. Note the absence of a third phase at the interface.

Figure 13 : Schematic representation of a unit cell of the $RE_2Fe_{14}B$ phase, situated at the grain boundary or the two-phase interface of a grain. For $x>0$, the environment consists of the oxygen stabilized fcc phase, while for $x<0$ it is the $RE_2Fe_{14}B$ phase. An oxygen atom at the interface is shown in order to depict possible interaction with Nd in the matrix phase.

Figure 14 : Applied field dependence of the intrinsic coercivity for (1) the water quenched sample ; (2) the water quenched +annealed sample ; (3) the slow cooled sample.

Schematic of Microstructure of Nd-Fe-B Magnets

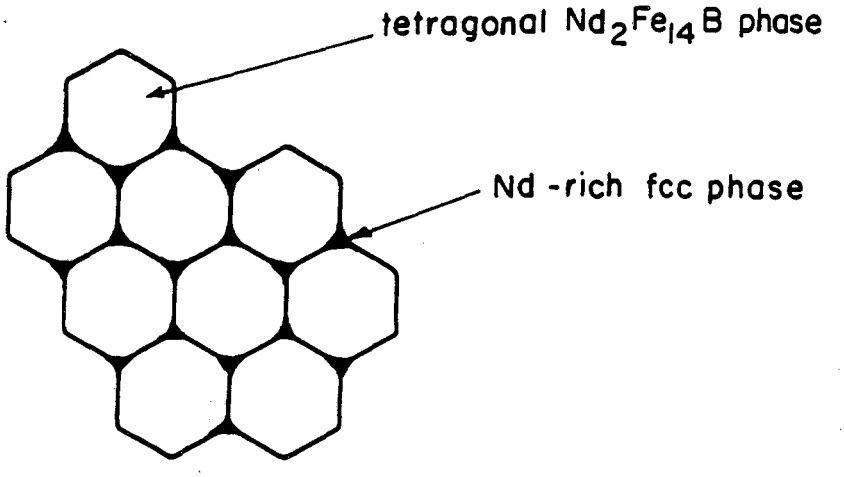

Figure 1

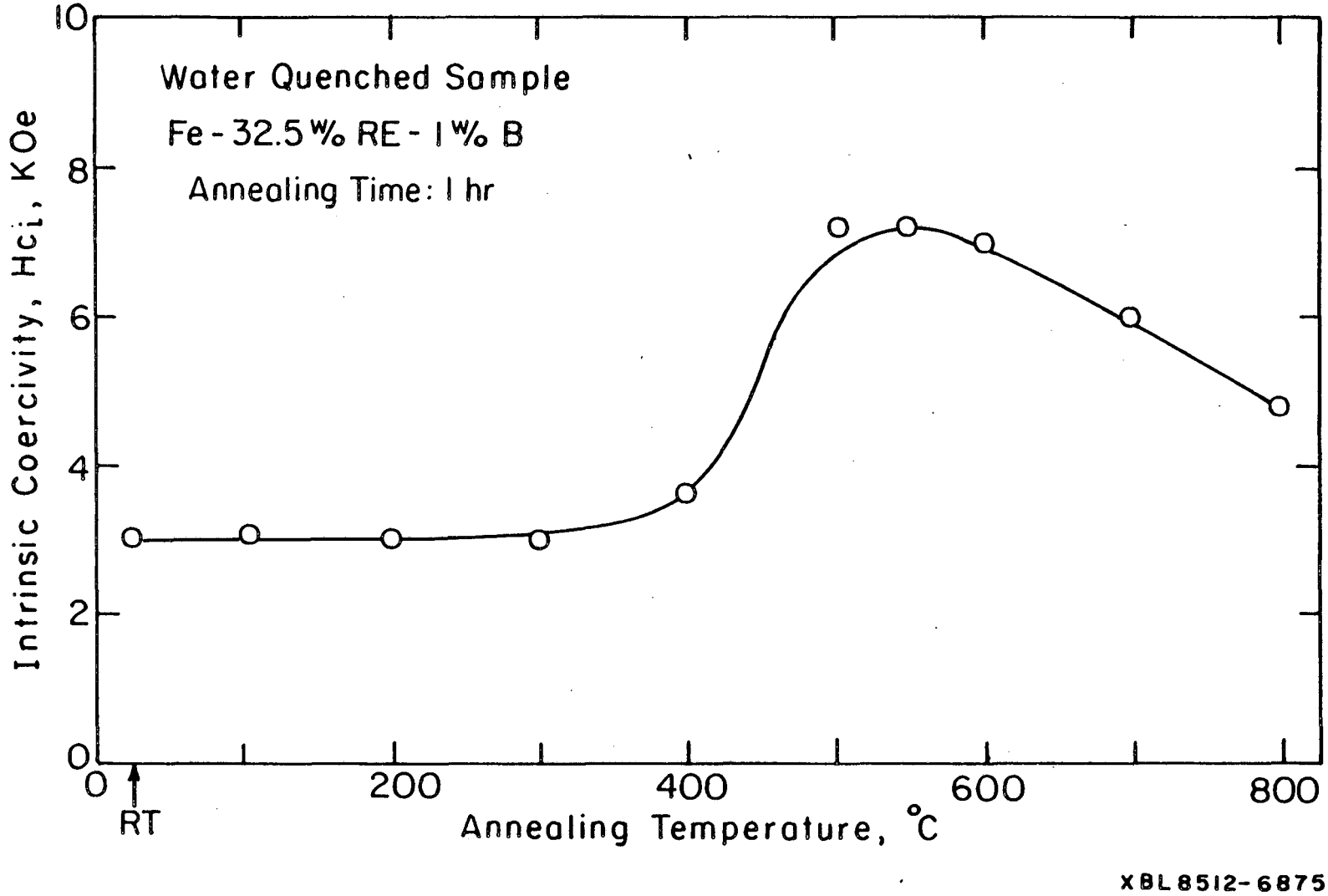
Water Quenched Sample
Fe - 32.5 w% RE - 1 w% B
Annealing Time: 1 hr
Intrinsic Coercivity, Hci, KOe
Annealing Temperature, °C
RT
0
2
4
6
8
10
0
200
400
600
800
XBL8512-6875

Figure 2

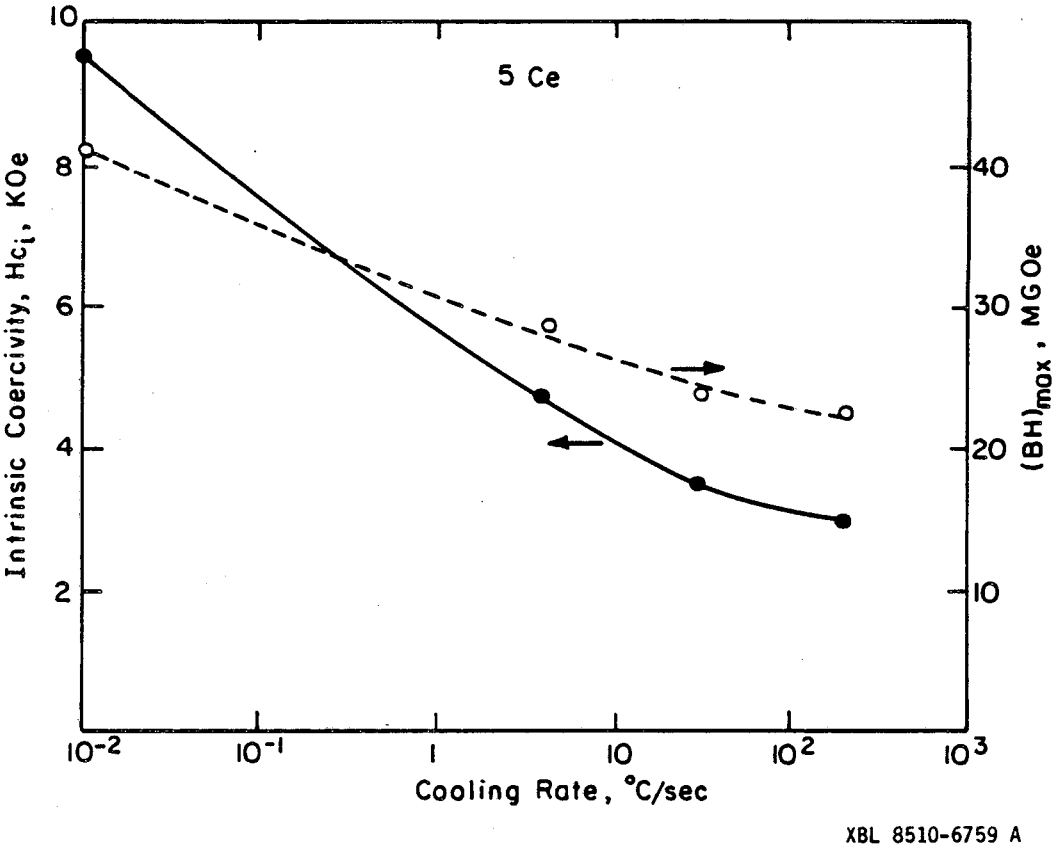
5 Ce
Intrinsic Coercivity, Hc_i, KOe
$(BH)_{max}$, MGOe
Cooling Rate, °C/sec
10
8
6
4
2
40
30
20
10
10^{-2}
10^{-1}
1
10
10^2
10^3
XBL 8510-6759 A

Figure 3

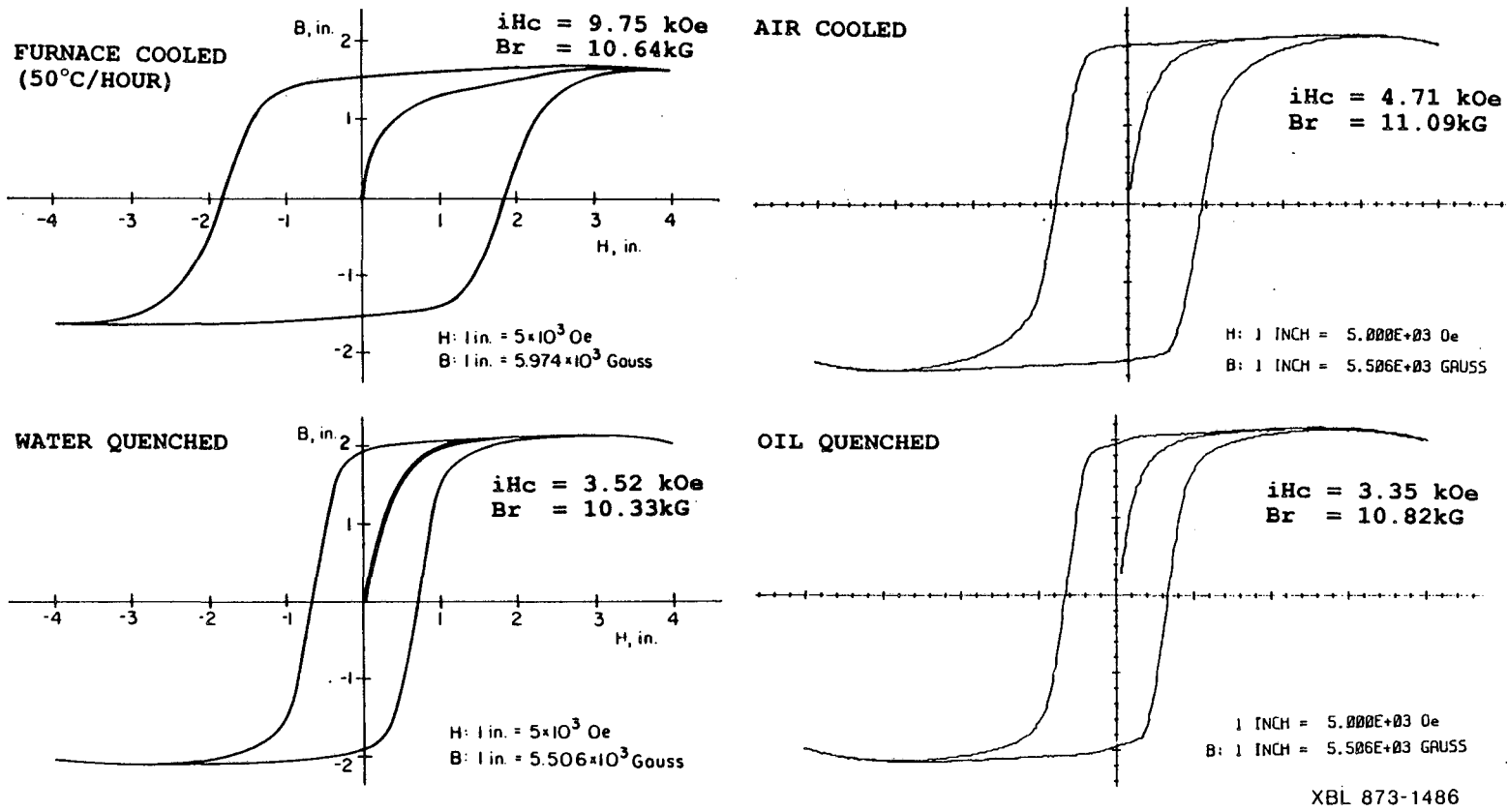
FURNACE COOLED
(50°C/HOUR)
iHc = 9.75 kOe
Br = 10.64kG
B, in.
H, in.
H: 1 in. = 5×10³ Oe
B: 1 in. = 5.974×10³ Gouss
AIR COOLED
iHc = 4.71 kOe
Br = 11.09kG
H: 1 INCH = 5.000E+03 Oe
B: 1 INCH = 5.506E+03 GAUSS
WATER QUENCHED
iHc = 3.52 kOe
Br = 10.33kG
H: 1 in. = 5×10³ Oe
B: 1 in. = 5.506×10³ Gouss
OIL QUENCHED
iHc = 3.35 kOe
Br = 10.82kG
1 INCH = 5.000E+03 Oe
B: 1 INCH = 5.506E+03 GAUSS
XBL 873-1486

Figure 4

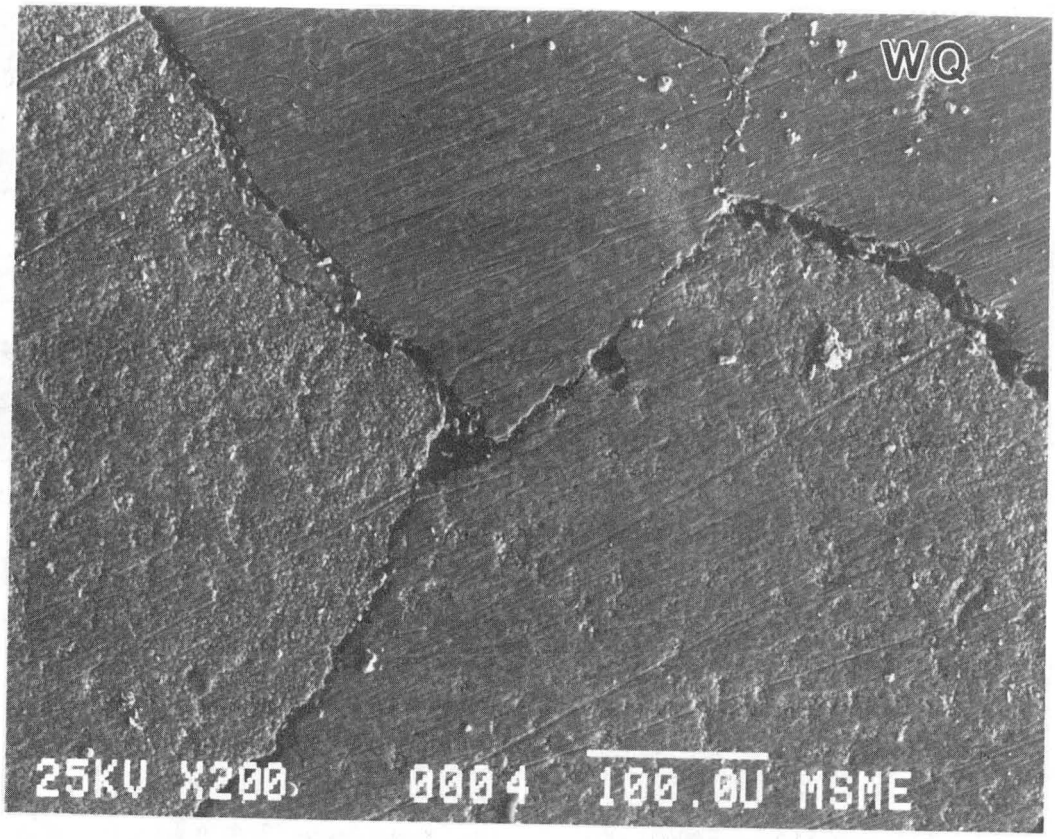

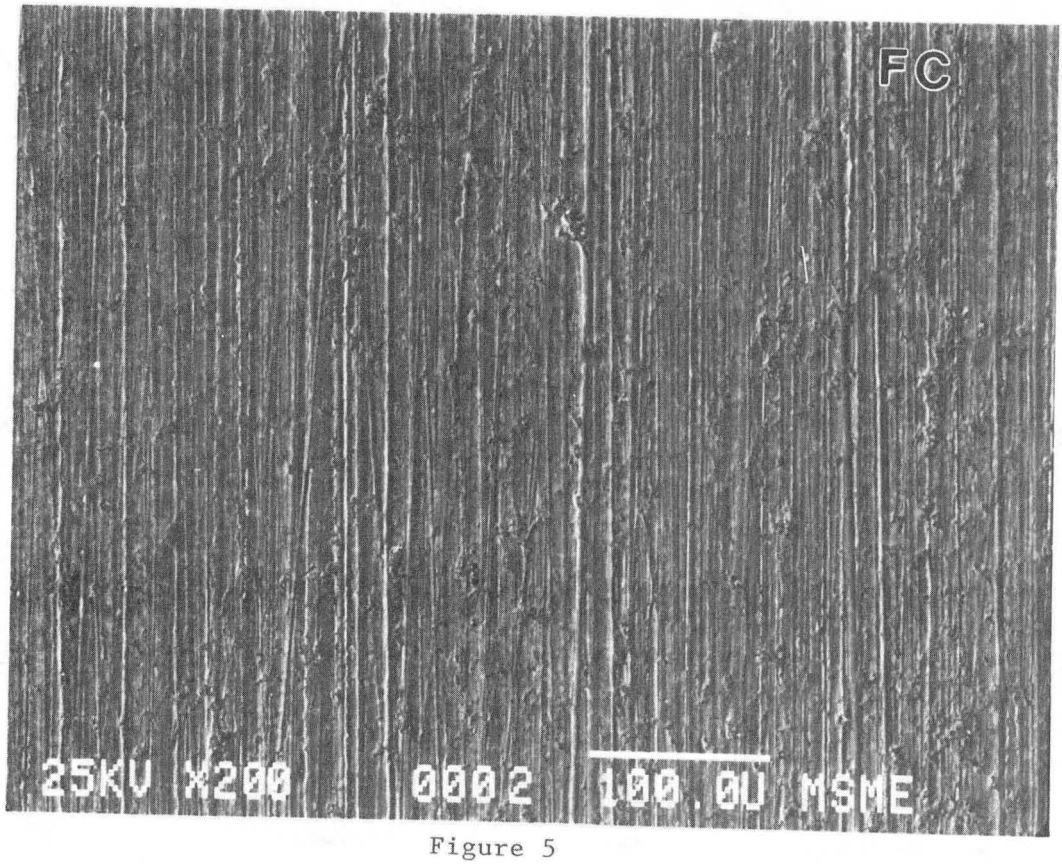

Figure 5

XBB 874-2629

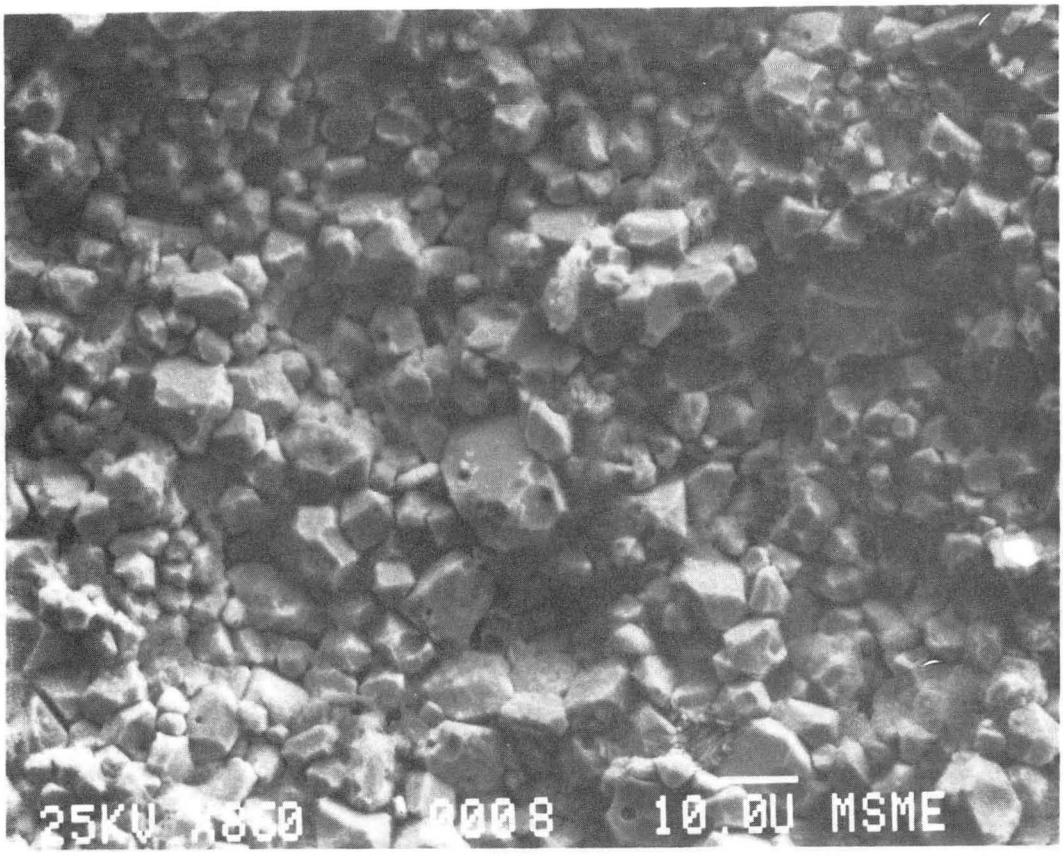

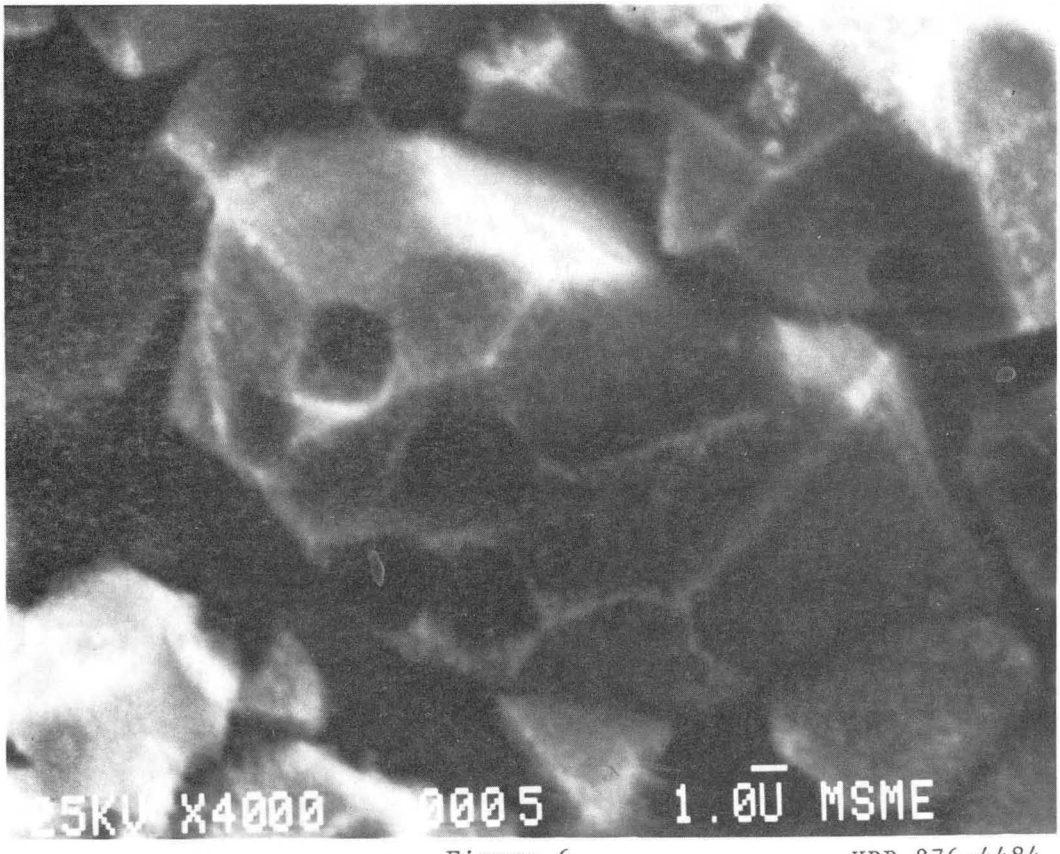

Figure 6 XBB 876-4484

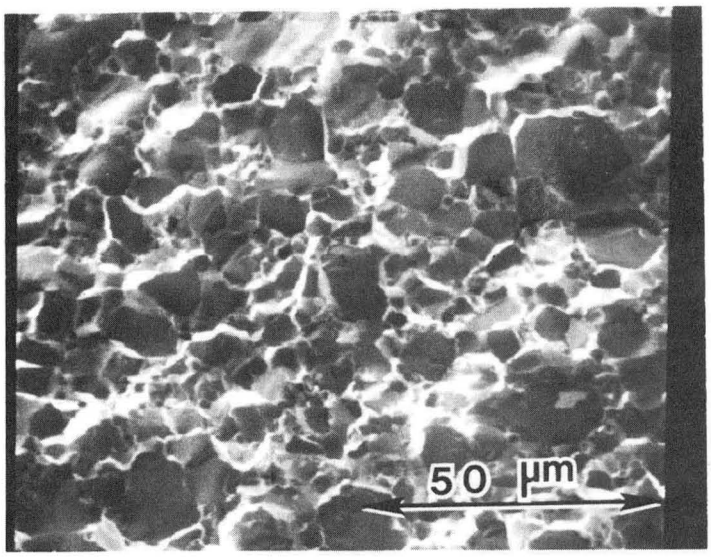

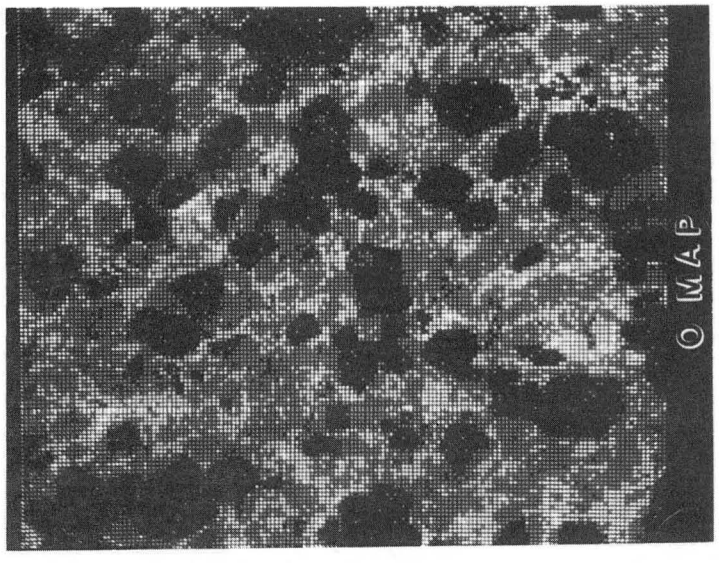

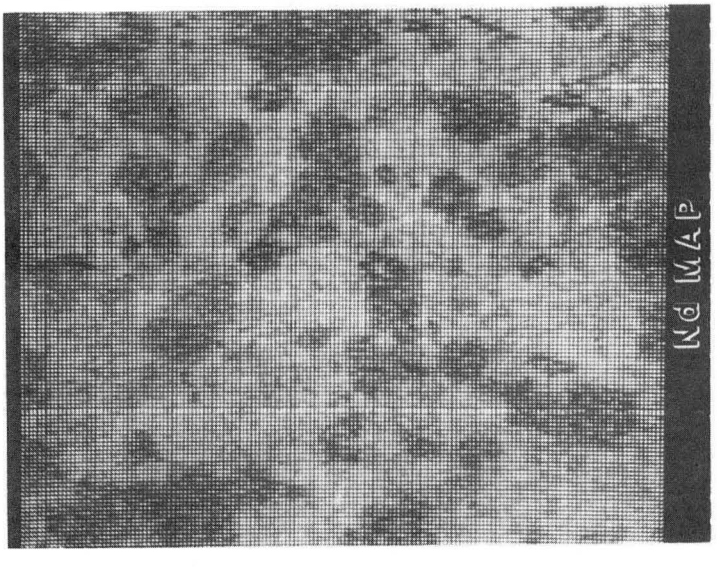

Figure 7

XBB 850-10300

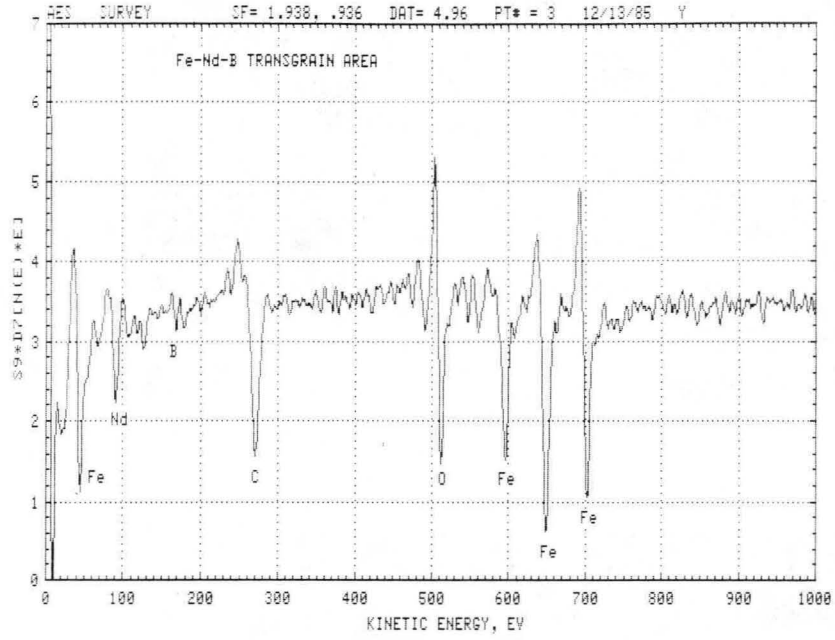

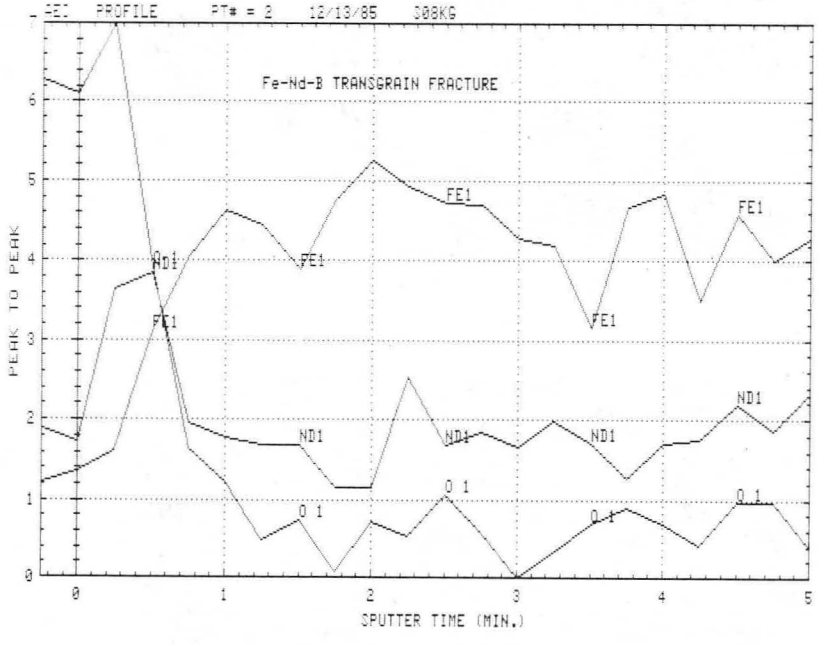

XBL 8512-5241

Figure 8

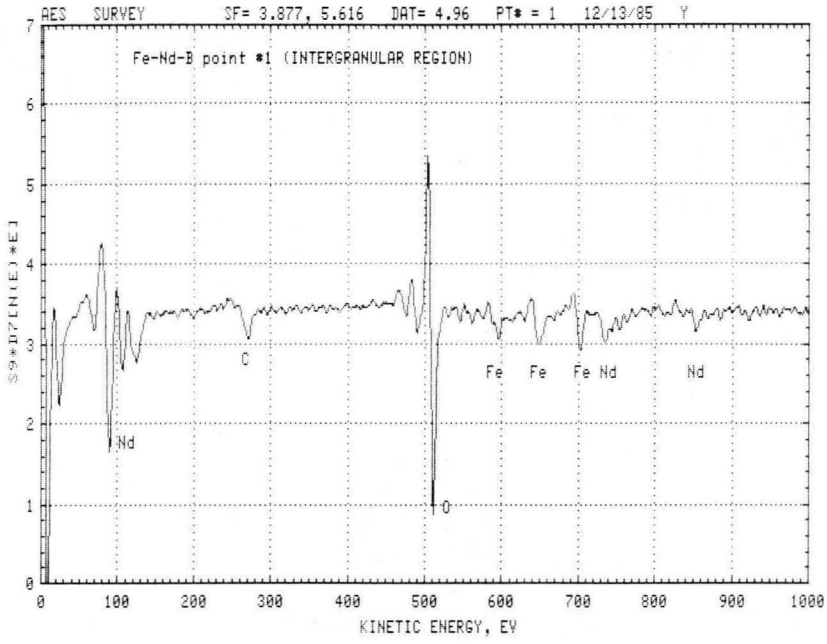

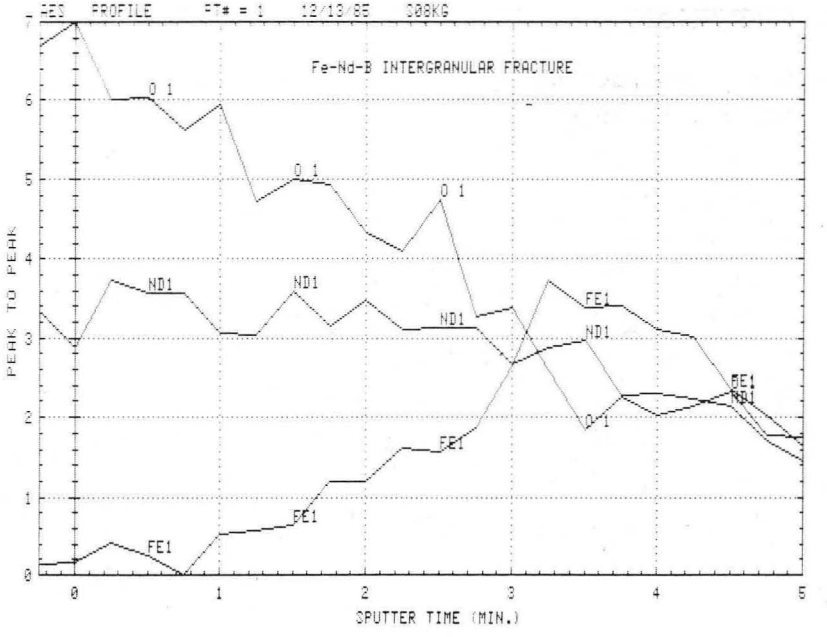

XBL 8512-5239

Figure 9

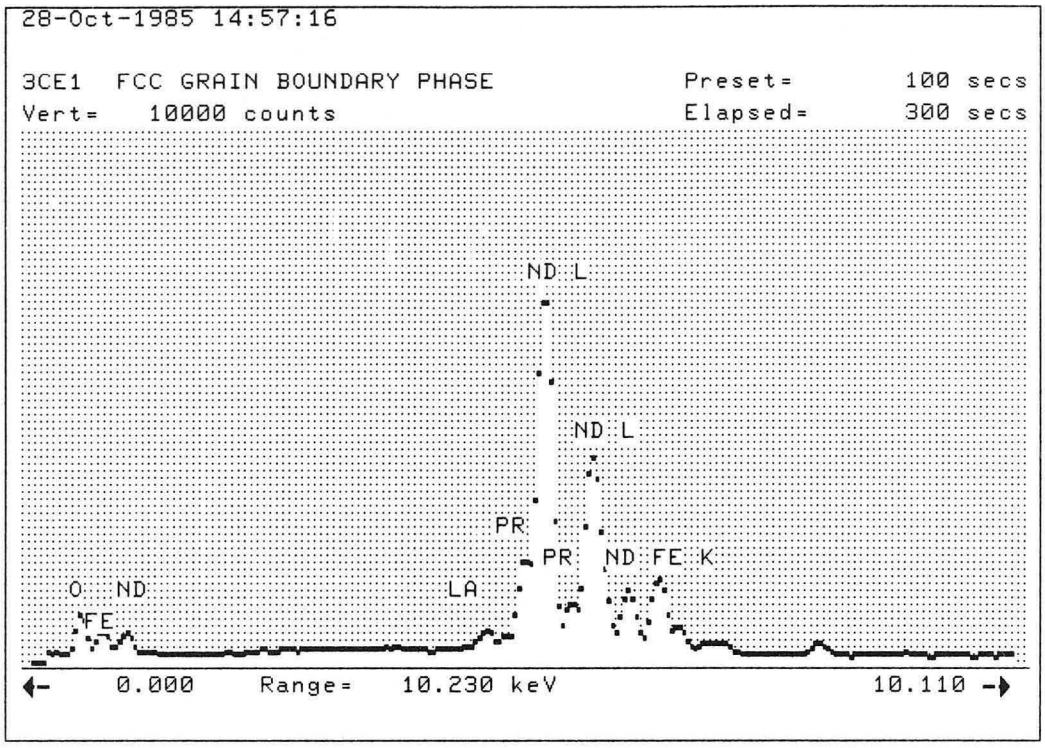

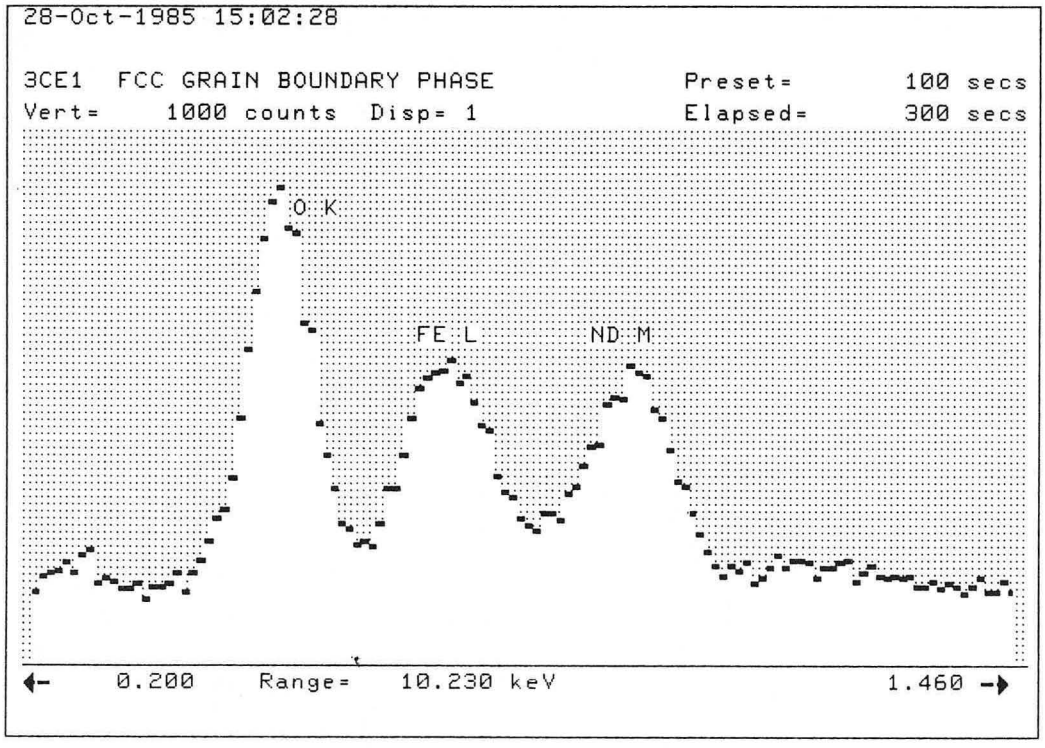

XBL 875-2254

Figure 10

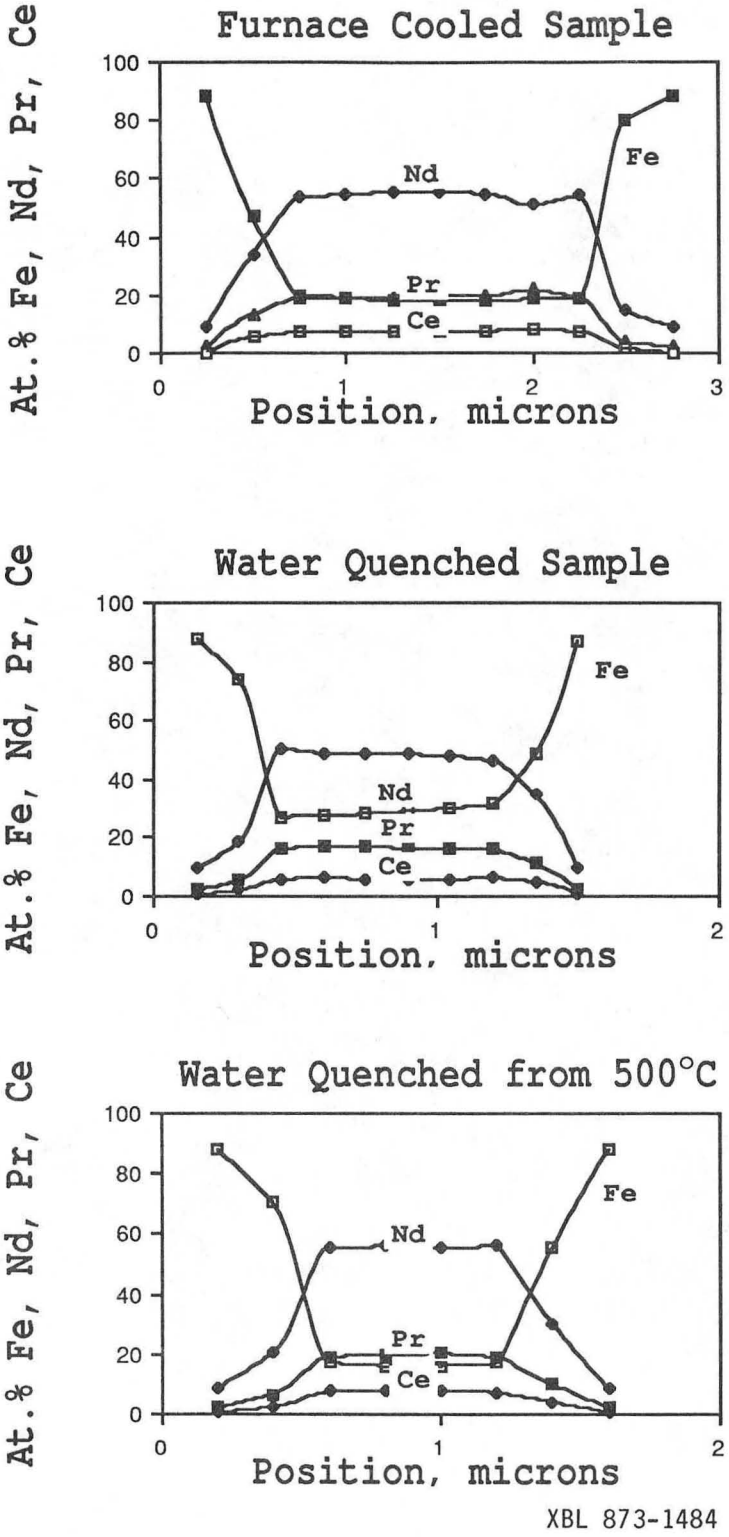
Furnace Cooled Sample
At.% Fe, Nd, Pr, Ce
100
80
60
40
20
0
Nd
Fe
Pr
Ce
0
1
2
3
Position, microns
Water Quenched Sample
At.% Fe, Nd, Pr, Ce
100
80
60
40
20
0
Fe
Nd
Pr
Ce
0
1
2
Position, microns
Water Quenched from 500°C
At.% Fe, Nd, Pr, Ce
100
80
60
40
20
0
Fe
Nd
Pr
Ce
0
1
2
Position, microns
XBL 873-1484

Figure 11

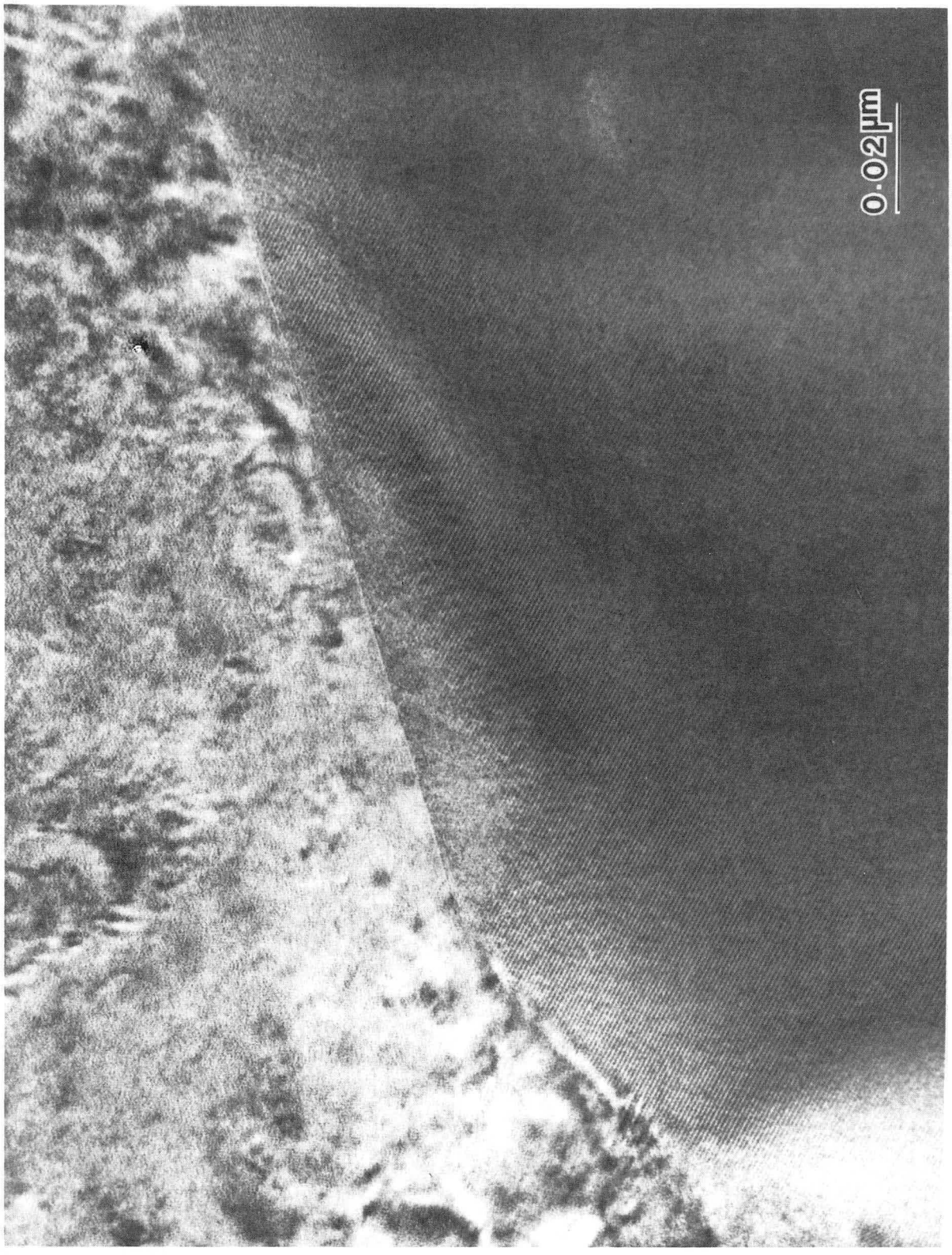

XBB 862-1436

Figure 12

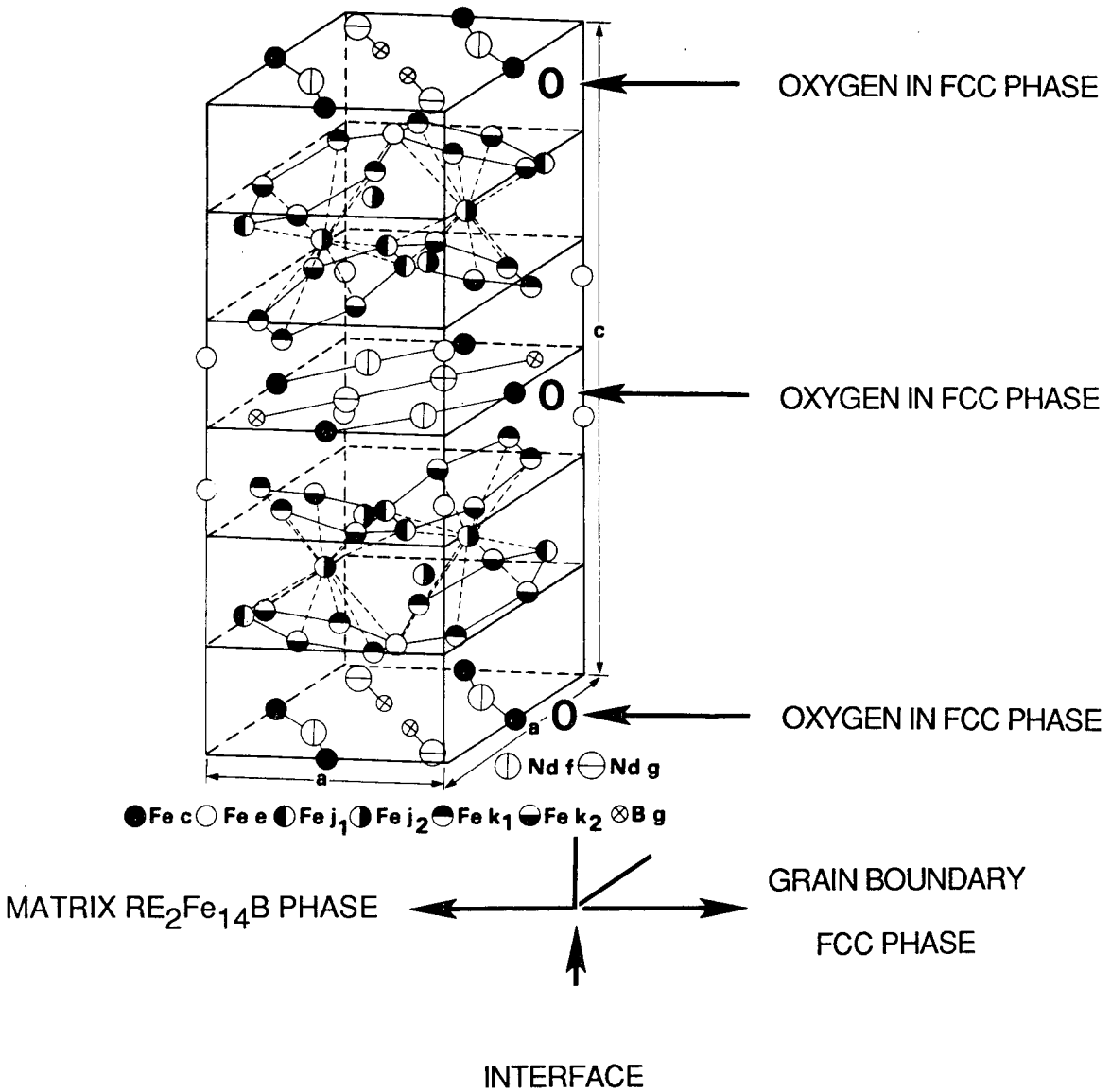

XBL 877-3362

Figure 13

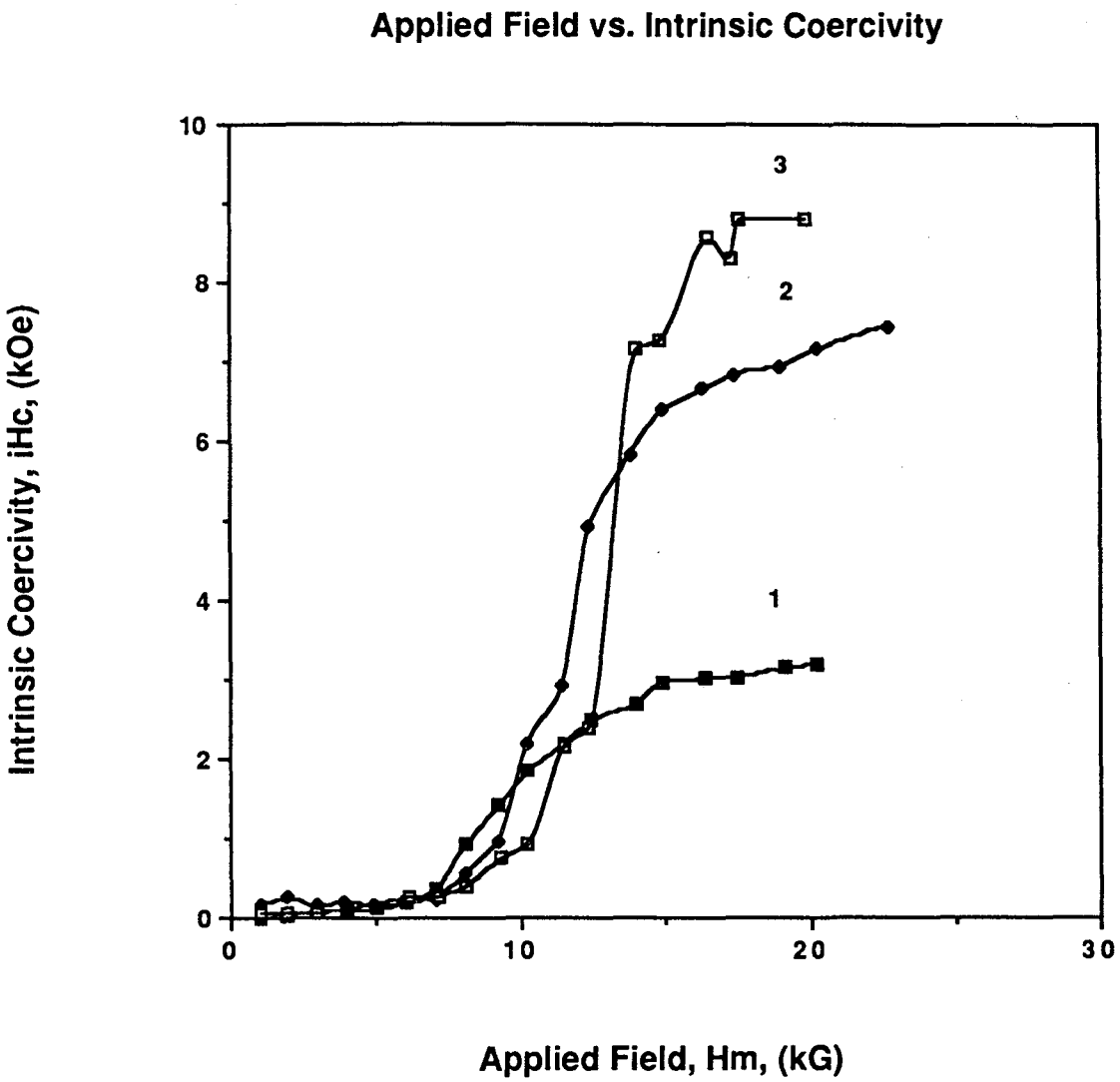
Applied Field vs. Intrinsic Coercivity
Intrinsic Coercivity, iHc, (kOe)
Applied Field, Hm, (kG)
10
8
6
4
2
0
0
10
20
30
3
2
1

Figure 14

LAWRENCE BERKELEY LABORATORY
TECHNICAL INFORMATION DEPARTMENT
UNIVERSITY OF CALIFORNIA
BERKELEY, CALIFORNIA 94720